



Article

# Alternatively Constructed Estrogen Receptor Alpha-Driven Super-Enhancers Result in Similar Gene Expression in Breast and Endometrial Cell Lines

Dóra Bojcsuk <sup>1,2,†</sup> , Gergely Nagy <sup>3,†</sup> and Bálint László Bálint <sup>1,\*</sup>

<sup>1</sup> Genomic Medicine and Bioinformatic Core Facility, Department of Biochemistry and Molecular Biology, Faculty of Medicine, University of Debrecen, 4032 Debrecen, Hungary; bojcsuk.dora@med.unideb.hu

<sup>2</sup> Doctoral School of Molecular Cell and Immune Biology, Faculty of Medicine, University of Debrecen, 4032 Debrecen, Hungary

<sup>3</sup> Department of Biochemistry and Molecular Biology, Faculty of Medicine, University of Debrecen, 4032 Debrecen, Hungary; nagygergely@med.unideb.hu

\* Correspondence: lbalint@med.unideb.hu

† These authors contributed equally to this work.

Received: 22 January 2020; Accepted: 25 February 2020; Published: 27 February 2020



**Abstract:** Super-enhancers (SEs) are clusters of highly active enhancers, regulating cell type-specific and disease-related genes, including oncogenes. The individual regulatory regions within SEs might be simultaneously bound by different transcription factors (TFs) and co-regulators, which together establish a chromatin environment conducting to effective transcription. While cells with distinct TF profiles can have different functions, how different cells control overlapping genetic programs remains a question. In this paper, we show that the construction of estrogen receptor alpha-driven SEs is tissue-specific, both collaborating TFs and the active SE components greatly differ between human breast cancer-derived MCF-7 and endometrial cancer-derived Ishikawa cells; nonetheless, SEs common to both cell lines have similar transcriptional outputs. These results delineate that despite the existence of a combinatorial code allowing alternative SE construction, a single master regulator might be able to determine the overall activity of SEs.

**Keywords:** estrogen receptor alpha (ER $\alpha$ ); transcription factor; enhancer; super-enhancer; MCF-7 cell line; Ishikawa cell line; ChIP-seq

## 1. Introduction

Estrogen receptor alpha (ER $\alpha$ ) is a well-studied member of the nuclear receptor (NR) superfamily and functions as a master regulator in several cell types, including breast, ovarian, and endometrial cancer cells [1–3]. The continuously changing level of its natural ligand, 17 $\beta$ -estradiol (E2), is indispensable for maintaining the ovarian cycle, and although normal hormone levels are responsible for female characteristics and contribute to healthy bone density among others, a higher estrogen/progesterone ratio in breast and endometrial tissues is linked to an increased risk of breast and endometrial cancer in postmenopausal women [4–6].

DNA binding by the receptor/ligand complex can occur directly through the estrogen response element (ERE) or via indirect protein-protein interactions [7–11]. According to previous studies, nearly one million EREs occur in the human genome, but only a small fraction of these EREs are located within open chromatin regions [12,13]. In addition, the number of EREs bound by ER $\alpha$  is reduced because the affinity of ER $\alpha$  for different EREs exhibits a broad spectrum [14]. High-affinity elements or canonical elements can immobilize the transcription factor (TF), thus exerting a much greater influence on gene expression than the weaker elements that most likely need other stabilizing TFs to generate

the activator complex or indirect DNA-protein interactions where an association with other TFs is required [15,16].

In the vicinity of highly expressed genes, multiple TFs are recruited to activate clusters of enhancers within a relatively small stretch of DNA, which are also known as super-enhancers (SEs) or clustered enhancers [17,18]. SEs can be characterized by a combination of active and open chromatin/enhancer marks, such as DNase I hypersensitivity, recruitment of the histone acetyltransferase P300, histone modifications such as acetylation at the lysine 27 residue of the histone H3 protein (H3K27ac), the chromatin modification reader BRD4 (a member of the bromodomain and extraterminal (BET) domain family) that recognizes acetylated histones, and MED1, which is one of the most important subunits of the Mediator complex that has a bridging role between enhancers and promoters via chromatin looping [19–21]. Recent studies reinforced that BRD4 and MED1 condensate at SEs in cell nuclei, and SE condensates can be isolated by liquid-liquid phase separation [22,23]. Interestingly, these protein clusters are assembled in a non-canonical way through the intrinsically disordered domains of their constituents, highlighting the importance of non-classical domain-based protein interactions, although according to several studies, SEs are located within CTCF-demarcated chromatin domains [24–27]. This phenomenon indicates that SEs concentrate the most important co-activator proteins, which distinguish them from typical enhancers. Although SEs can make physical contact with their target promoters from very long distances, these are mostly identified near cell type-specific or disease-related genes, which act as determinants of cell identity [17,24]. As suggested by several studies on cancer cells, SEs contribute to the expression of relevant biomarker genes that might be used for targeted therapeutic development; however, numerous questions regarding their exact gene regulatory functions remain unanswered [28,29].

We previously presented that the formation of ligand-inducible ER $\alpha$ -driven SEs depends on the presence of canonical EREs, which can initiate further ER $\alpha$  binding events at nearby and even less specific binding sites [15,16]. These primary “mother” or “hub” enhancers (a term coined by Huang et al.) represent active chromatin regions even in the absence of specific treatment, and these form the basis of ligand-inducible SEs [30]. In the present study, we investigated whether (i) ER $\alpha$ -driven SEs develop around the same canonical elements or in the same genomic regions in different cancer cell lines, and also studied (ii) the common and (iii) cell line-specific characteristics of these SEs. Furthermore, we examined in detail whether (iv) the effect of SEs on gene expression is equivalent in two inherently different cancer cell lines. In order to answer these questions, by using publicly available chromatin immunoprecipitation followed by sequencing (ChIP-seq) data, we predicted ER $\alpha$ -driven SEs in human breast cancer-derived MCF-7 and endometrial cancer-derived Ishikawa cell lines in which ER $\alpha$  is a key master regulator. We raised the possibility that comprehensive characterization of cell line-specific ER $\alpha$ -driven gene regulatory units may also be important in understanding how ER $\alpha$ , as a master TF can fine-tune different cell functions in a way that a core set of SEs can retain the same function with different regulatory elements in different tissues.

## 2. Results

### 2.1. General Comparison of the Putative ER $\alpha$ Binding Sites in MCF-7 and Ishikawa Cells

Comparing different cell types, enhancers show an extremely high level of variability [31]. By testing the similarities between MCF-7 and Ishikawa cells at the level of ER $\alpha$  cisomes upon E2 treatment, we found that both cell lines had tens of thousands of ER $\alpha$  transcription factor binding sites (TFBSs), but most of these sites were characteristic of only one of the investigated cell lines (Figure 1A). This cell line-specific and overlapping ER $\alpha$  binding pattern is also followed by the presence of H3K27ac signals suggesting that there is a large difference between the chromatin accessibility in the two investigated cell lines (Figure 1B). In line with this result, EREs, which were commonly occupied by ER $\alpha$  in both cell lines, showed the highest motif scores, followed by those of MCF-7-specific and then Ishikawa-specific sites (Figure 1C). Based on our previous findings, these results suggest that a

subset of EREs among commonly used EREs might be considered common nucleating sites of SEs and in Ishikawa cells, the lower affinity of ER $\alpha$ -occupied EREs requires the assistance of collaborating factors [15,16].

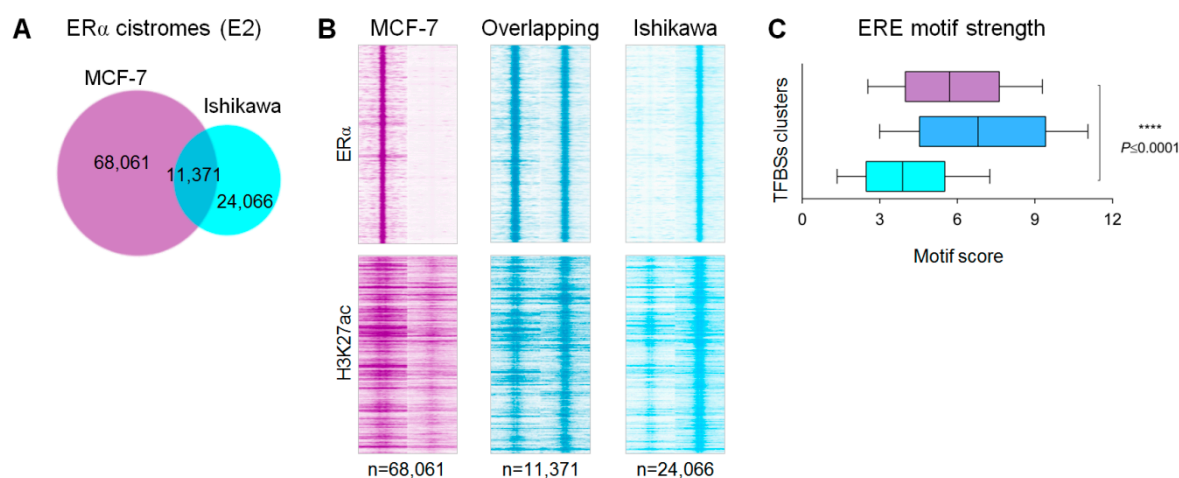


**Figure 1.** Genome-wide comparison of ER $\alpha$  cistromes and transcriptomes in MCF-7 and Ishikawa cells upon E2 treatment. **(A)** Area-proportional Venn diagram showing the overlap between all ER $\alpha$  TFBSs upon E2 treatment in MCF-7 and Ishikawa cells. **(B)** Read distribution plots showing the presence or absence of the identified cell line-specific and overlapping ER $\alpha$  TFBSs and the H3K27ac signals in 2-kb frames. **(C)** Box plots showing the ERE motif strength within the summit  $\pm 100$ -bp region of the shared and cell line-specific TFBSs, defined in Figure 1A. The boxes represent the first and third quartiles, the lines indicate the median scores and the whiskers indicate the 10th to 90th percentile ranges. Unpaired t-test, \*\*\*\* significant at  $p < 0.0001$ .

## 2.2. ER $\alpha$ -driven SE Constituents have Different Motif Preferences in MCF-7 and Ishikawa Cells

In accordance with the preliminary findings showing that a subset of enhancers are commonly occupied by ER $\alpha$  in both cell lines, we narrowed our focus on how ER $\alpha$ -driven SEs in different TF environments are assembled; therefore, we assessed ER $\alpha$  binding sites at the SE regions specific for MCF-7 and Ishikawa cells. Importantly, some studies define SEs based on H3K27ac or MED1 signals; here we consider this approach based on the binding density of ER $\alpha$ . We predicted 392 SE regions in MCF-7 and 618 in the Ishikawa cell line respectively, and most of their constituents were characteristic of only one investigated cell line (Figure 2A, Supplementary Figure S1A,B and Table S1A). The cell line-specific, ER $\alpha$ -driven SE constituents were  $\sim 3.4$  times more abundant in MCF-7 ( $n = 3872$ ) and  $\sim 1.9$  times more abundant in Ishikawa ( $n = 2138$ ) cells than those present in both cell lines ( $n = 1124$ ) (Figure 2A, Supplementary Figure S1B). The presence of DNase I hypersensitivity, H3K27ac and P300 also followed the three well-separated binding patterns (Supplementary Figure S1C and Table S1B). The resulted “clusters” were referred to as: (1) MCF-7-specific, (2) shared, as they are common to both cell types, and (3) Ishikawa-specific, highlighted if possible in blue, purple, and red, respectively, in the figures.

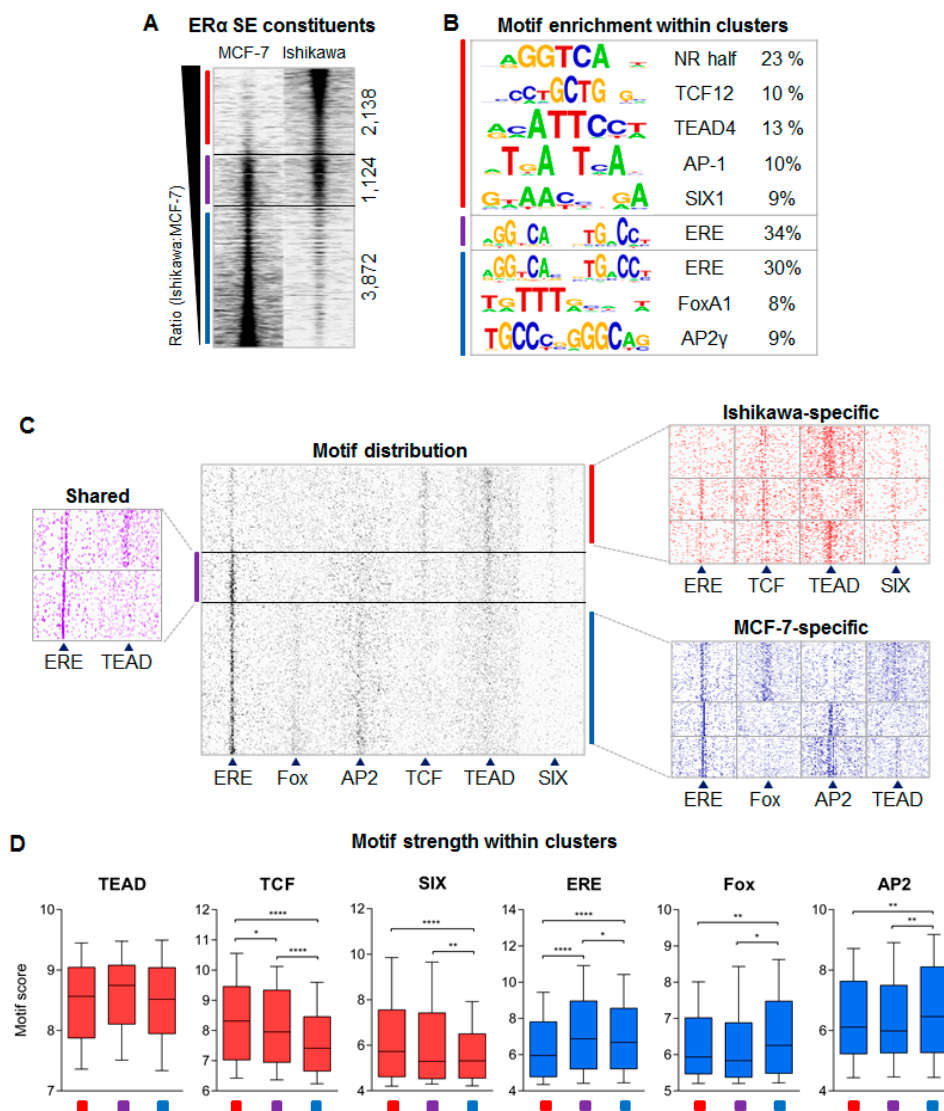


**Figure 2.** ER $\alpha$ -driven super-enhancer constituents show distinct binding patterns and motif preferences in MCF-7 and Ishikawa cells. (A) Read distribution plot showing ER $\alpha$  density on ER $\alpha$ -driven super-enhancer (SE) constituents derived from MCF-7 and Ishikawa cells in 2-kb frames. Peaks were sorted based on the ratio of RPKM (reads per kilobase per million mapped reads) values calculated from Ishikawa and MCF-7 cells and were separated into three different clusters: the red line represents Ishikawa-specific constituents ( $n = 2138$ ), the purple line represents shared constituents ( $n = 1124$ ), and the blue line represents MCF-7-specific SE constituents ( $n = 3872$ ). (B) The enriched motifs and their percentages within the target regions of the three clusters. (C) The motif distribution plot of ERE, Fox, AP2, TCF, TEAD, and SIX motifs in 1.5-kb frames around the summit position of ER $\alpha$ -driven SE constituents in the same order as introduced in Figure 2A (middle). Colored heat maps represent shared and cell line-specific clusters when peaks were further clustered based on the presence or absence of the most frequent motifs. (D) Box plots showing the distribution of motif strengths within the three main clusters introduced in Figure 2A. The boxes represent the first and third quartiles, the horizontal lines indicate the median scores and the whiskers indicate the 10th to 90th percentile ranges. Paired t-test, \* significant at  $p < 0.05$ , \*\* at  $p < 0.01$ , \*\*\* at  $p < 0.001$ , \*\*\*\* at  $p < 0.0001$ .

The first substantial difference observed between the three identified clusters was seen in their enriched DNA motifs (Figure 2B, Supplementary Figure S1D). Within the commonly occupied TFBSs, only the ERE and different direct repeats (DRs) of the nuclear receptor half-site (NR half) were enriched, whereas, in the cell line-specific clusters, motifs of other TFs could also be identified. Specifically,

motifs of the Fox and AP2 proteins were enriched in the MCF-7-specific cluster, and motifs of the TEAD, TCF, AP-1, and SIX proteins were enriched in the Ishikawa-specific cluster. The latter cluster did not show enrichment of the ERE motif but only the more general NR half-site, which suggests that in the Ishikawa-specific sites ER $\alpha$  needs the assistance of its co-factor(s).

In MCF-7 cells, in addition to ER $\alpha$ , forkhead box A1 (FoxA1) is the most influential TF and is present in approximately half of ER $\alpha$ -bound genomic regions even in the absence of E2 [32,33]. FoxA1 plays a role as a pioneer factor of ER $\alpha$ , thus facilitating its binding, while activator protein 2 gamma (AP2 $\gamma$ ), another major TF, stabilizes the DNA-protein interaction [34]. Although GATA binding protein 3 (GATA3) and retinoic acid receptor alpha (RAR $\alpha$ ) were also identified as ER $\alpha$  cooperative factors in breast cancer cells, these were not identified as crucial players in our investigations on ER $\alpha$ -driven SEs [15,35–37].

All TF families that had their motifs enriched at the sites bound by ER $\alpha$  identified in Ishikawa cells were previously directly associated with ER $\alpha$  in endometrial cancer [38]. TEA domain transcription factor 4 (TEAD4) cooperates with activator protein 1 (AP-1) in the chromatin of endometrial cancer cells and establishes an interaction between ER $\alpha$  and progesterone receptor (PR) in breast cancer cells [39,40], transcription factor 12 (TCF12), also known as HEB, functions as an oncogene as well as a tumor suppressor in several human cancer types [41]. In mouse experiments, TCF12 was also identified as a key prognostic factor for endometrial cancer [42]. Although all of the above-mentioned endometrial cancer-related proteins follow the binding of ER $\alpha$  in Ishikawa cells, there are no reports on these proteins regarding ER $\alpha$ -driven SEs. Furthermore, the elevated expression of SIX1 is a biomarker of hyper- or dysplastic cells in human endometrial cancers [43]. The exclusivity of the motifs in the cell line-specific clusters suggested a different mode of action between the SEs and the assembled TF complexes of our two chosen models where ER $\alpha$  is present as a master regulator.

Based on these initial findings, we carried out a detailed investigation of how different TFs contribute to the formation of both cell line-specific and shared ER $\alpha$ -driven SEs. First, for validation, we mapped the matrix of the identified DNA motifs and found that the shared ER $\alpha$  binding sites showed large numbers of ERE and smaller numbers of other elements, whereas the cell line-specific enhancers showed expected motif distribution patterns: Fox and AP2 motifs were enriched at MCF-7-specific ER $\alpha$  binding sites, while TCF, TEAD, and SIX motifs were enriched at Ishikawa-specific ER $\alpha$  binding sites (Figure 2C, Supplementary Figure S2A). Further dividing the three clusters based on motif distribution showed that certain motifs (e.g., ERE and TEAD or Fox and AP2) mutually exclude each other (Figure 1C). In order to examine the strengths of the enriched motifs, we plotted the motif scores within the cell line-specific and shared clusters (Figure 2D, Supplementary Figure S2B).

Generally, motif strengths correlated well with motif distribution patterns; however, TEAD motifs did not show significantly different motif strengths between the analyzed clusters ( $p > 0.05$ ; not significant). These results indicated that the two cell lines use different sets of TFs and that motif distribution within SEs may represent a DNA-encoded component of SE-driven transcription regulation.

### 2.3. Response Elements Determine the Hierarchy between FoxM1/TCF12/TEAD4 Proteins in Ishikawa Cells

As TF motifs may be bound by several proteins of a TF family, we compared the expression levels of all members of the emerging TF families from publicly available RNA-seq data sets. In addition to *FOXA1* and *TFAP2C* (encoding AP2 $\gamma$ ), *ESR1* (encoding ER $\alpha$ ) also showed much lower expression in Ishikawa cells than in MCF-7 cells. This result is consistent with the less prominent dominance of ER $\alpha$  in Ishikawa cells than in MCF-7 cells and partially consistent with substitution or supplementation of its function by other TFs (Figure 1B). Of the more than 40 members of the Fox family, *FOXM1* had the highest expression in Ishikawa cells; however, *FOXD1* also showed a notable expression level (Supplementary Figure S3A,B and Table S1B). Based on previous studies, in Ishikawa cells, forkhead box M1 (FoxM1) and CCAAT/enhancer-binding protein beta (C/EBP $\beta$ ) were also described as potential regulatory partners of ER $\alpha$  [38]. Although the C/EBP motif—similarly to the Fox motif—is not a typical component of ER $\alpha$ -driven SEs, previous studies suggest that C/EBP $\beta$  can stabilize ER $\alpha$  in a

DNA binding complex; therefore, we plotted the gene expression levels of the whole gene family (Supplementary Figure S3C) [44]. *TCF12* and *TEAD4* showed higher expression in Ishikawa cells than in MCF-7 cells, but this pattern was also observed for other family members, such as *TCF3* and *TEAD2*. Although *SIX* genes were expressed at low levels in both cell lines, *SIX5* was expressed at higher levels in Ishikawa cells, and *SIX4* was specific to MCF-7 cells. Of all these genes, *CEBPB* showed the highest expression, and the genomic distribution of its protein product as investigated by TF mapping followed the binding pattern of ER $\alpha$  even in the absence of ligand treatment in Ishikawa cells (Supplementary Figure S3D); therefore, we included it in additional analyses. In accordance with the absence of any C/EBP motif enrichment in our previous results (Figure 2B, Supplementary Figure S1E), we could not detect any C/EBP motif enrichment around the ER $\alpha$  SE constituents (Supplementary Figure S3E). At these sites, similar to FoxM1, C/EBP $\beta$  may bind indirectly to the DNA through ER $\alpha$  or other DNA binding collaborators less affected by E2 treatment. Together with all of the above-mentioned TFs, C/EBP $\beta$  followed cell line-specific ER $\alpha$  binding patterns (Supplementary Figure S3D,F). The gene expression comparison confirmed the role of collaborating TFs and highlighted FoxM1 as a TF with a major role in Ishikawa cells.

In addition, by examining the overall binding of specific TFs to DNA as expressed in average RPKM values per motif distribution-based sub-clusters defined in Figure 2C, we identified specific patterns of protein co-occurrences. All TFs showed high density at their specific elements and to a lesser extent, other TFs were also recruited, except for FoxA1 and AP2 $\gamma$ , which excluded each other's presence at MCF-7-specific sites (Figure 3A). Unsurprisingly, the recruitment of ER $\alpha$  upon E2 treatment was observed in each sub-cluster even at binding sites that lacked ERE (Figure 3A, Supplementary Table S1B).

In order to closely examine the protein-protein interactions suggested by these results, we performed a correlation analysis on TF binding (Figure 3B). In Ishikawa cells, FoxM1 and TCF12 showed the strongest co-occurrence with each other and with TEAD4 and E2-induced ER $\alpha$ . Although C/EBP $\beta$  could be detected at ER $\alpha$ -driven SE constituents, its density did not show any correlation with ER $\alpha$  binding; instead, its density was correlated with the Ishikawa-related FoxM1/TCF12/TEAD4 protein trio. The correlation heat map for MCF-7 suggested more independent recruitment of key TFs.

In order to examine both protein-protein and DNA-protein concomitance, we plotted TF densities at their putative TFBSs (Figure 3C, Supplementary Figure S4A,B). This type of representation clearly visualized that different TFs show higher density at their own elements, and we also obtained information about their co-occurrence with each other at the same genomic sites. In Ishikawa cells, the presence of ER $\alpha$  correlated best with that of FoxM1, followed by co-occurrence with TCF12 and TEAD4. Pairwise comparisons suggested a FoxM1/TCF12, TCF12/TEAD4, and FoxM1/TEAD4 interaction, which implies a tripartite complex interacting with ER $\alpha$  (Figure 3C,D, Supplementary Figure S4A,B). The TCF12/TEAD4 relationship was also reproduced even with lower protein levels in MCF-7 cells ( $r = 0.8833$ ) (Supplementary Figure S4B). C/EBP $\beta$  binding showed no or only weak correlation ( $r = 0.3489$ ) with other TFs except for FoxM1; however, the low number of response elements could cause a bias towards their interaction (Supplementary Figure S4A). Contact between a steroid hormone receptor and Fox protein is not unprecedented as androgen receptor (AR) and FoxA1 associate to occupy ARE::Fox composite elements. However, a single ARE or Fox motif is usually sufficient for binding by both proteins [45–47]. In our proposed mechanism, any TF can bind its DNA element, and this process is sufficient for anchoring the entire complex of proteins. As Ishikawa-specific Fox motifs are very rare (as shown on Figure 2C), FoxM1 is typically not a direct DNA binder. This finding also indicates no need for direct DNA binding by ER $\alpha$  for regulation in Ishikawa cells (unlike our previously described finding in MCF-7 cells) (Figure 3A,B). In MCF-7 cells, there was no close correlation between dominant proteins, and ER $\alpha$ /FoxA1 concomitances seemed to be the least frequent ( $r = 0.3626$ ). Upon E2 treatment, we observed a slight recruitment of FoxA1 and stronger recruitment of AP2 $\gamma$ , which was previously described (Supplementary Figure S4B). In a few TFBSs, two motifs could be mapped (green dots); these regions were usually bound by their specific TFs to a similar extent.

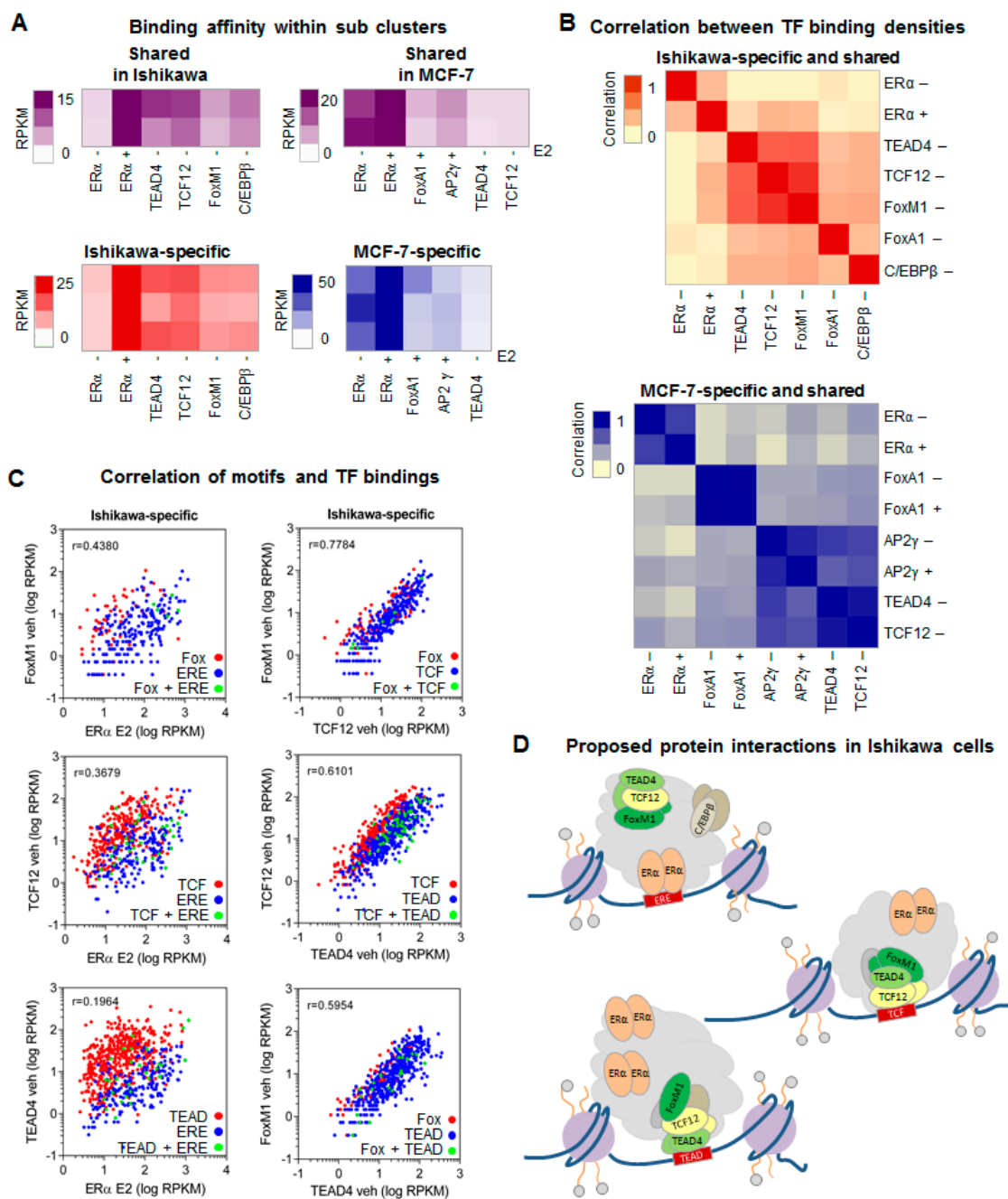


**Figure 3.** Response elements determine a consistent hierarchy between transcription factor binding events. (A) Heat maps depict the density of relevant TFs in the presence (+) or absence (−) of E2 within the same sub-clusters introduced in Figure 2C. The plotted densities are the averages of the values calculated by HOMER within 50-bp regions around the summit of the sub-clusters’ SE constituents. In the case of shared peaks, ChIP-seq coverages were separately calculated for both Ishikawa and MCF-7 cells. (B) Correlation plots showing the correlation coefficients (r) calculated from the densities of all investigated TFs on the SE constituents (summit ± 50-bp regions) of Ishikawa and MCF-7 cells. (C) Scatter plots showing the densities of the indicated TFs (upon vehicle [veh] or E2 treatment) on their DNA binding motifs within the MCF-7- or Ishikawa-specific ERα-driven SE constituents. Red and blue dots represent protein binding on a specific single motif, and green dots represent protein binding on a region with the motifs of both examined TFs. (D) Working models of the supposed hierarchy between ERα, FoxM1, TCF12, and TEAD4 TFs in Ishikawa cells based on the presence of ERE, TCF, or TEAD response elements.

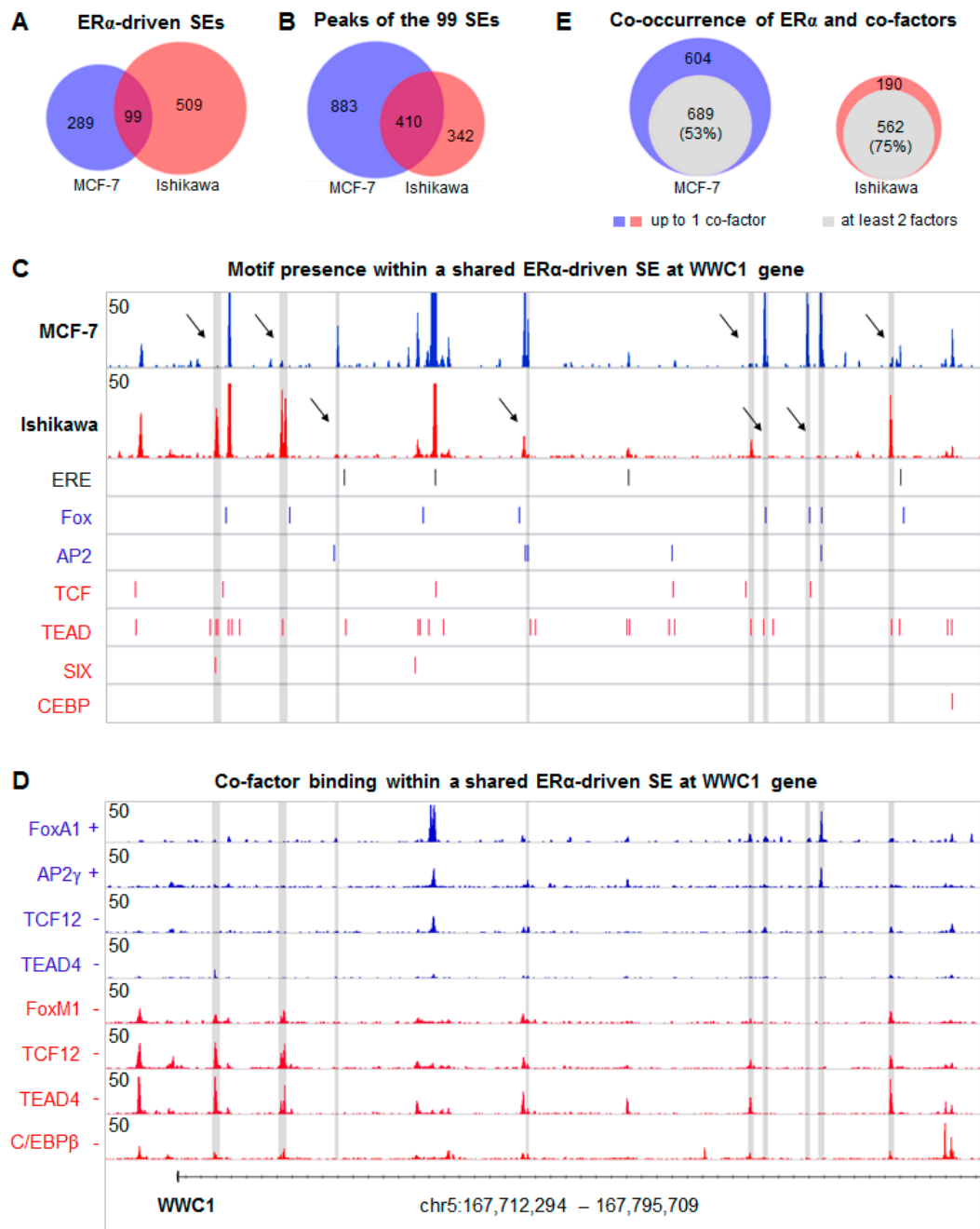
Together, these findings indicated that TF binding events followed the DNA motif pattern and that well-defined cooperativity and hierarchy existed between TFs promoting the formation of complexes on SEs.

#### 2.4. Overlapping SE Regions Are Composed of Different ER $\alpha$ Binding Sites

By focusing on complete ER $\alpha$ -driven SE regions, we found 99 SEs that partly or fully overlapped between MCF-7 and Ishikawa cells. Nonetheless, these “common” SEs shared only a quarter of their ER $\alpha$  TFBSs (410 in total) (Figure 4A,B, Supplementary Figure S5A). This heterogeneity of SE composition, which was also observed at the *WWC1* locus, suggests a strong cell type- and TF-specific enhancer usage. For instance, despite its lower expression in MCF-7 cells, TCF12 was significantly recruited to the central constituent of the SE, carrying an ERE and TCF motif (Figure 4C,D). This representative region clearly demonstrated how Ishikawa-specific factors localized together and how their TFBSs were separated from those of MCF-7-specific TFs (Figure 4D). Moreover, in Ishikawa cells, ER $\alpha$  mostly occupied binding sites together with its collaborating factors. By contrast, in MCF-7 cells, ER $\alpha$  binding events were much more isolated.

In order to measure the extent of ER $\alpha$  autonomy, we compared the number of SE constituents bound by at least two collaborating TFs that were present in MCF-7 or Ishikawa cells (Figure 4E). Within the 99 shared SEs, 47% of MCF-7-specific and 25% of Ishikawa-specific SE constituents were bound by a maximum of one TF other than ER $\alpha$ , which implies that in Ishikawa cells ER $\alpha$  typically requires several collaborating TFs for effective binding, while in MCF-7 cells this is optional. Another tendency observed at the *WWC1* locus was the opposed binding strength between ER $\alpha$  and its collaborating factors in Ishikawa cells (Figure 4C,D). In order to test this finding, we sorted protein densities by the ratio of ER $\alpha$  and TEAD4 signals (Supplementary Figure S5B). Indeed, the strongest ER $\alpha$  peaks were mostly established on EREs and typically lacked collaborating factors, while co-occurrence with strong cofactor binding resulted in moderate recruitment of ER $\alpha$ . This was in agreement with the results of correlation analyses, indicating the significance of DNA-protein and protein-protein interactions (Figure 3C, Supplementary Figure S4A). In the case of MCF-7-specific TFs, we observed a high ratio of direct ERE binding and a positive correlation between protein enrichments (Supplementary Figure S5C). Altogether, these results also supported our model (Figure 3D), showing that DNA binding by even one of the examined TFs was able to promote the recruitment of other TFs that might be part of a cell line-specific protein complex.

In general, we found only one or two putative response element(s) per peak, and in some cases, none of the motif matrices used could be identified (Figure 4C). Within the common SE regions, the shared binding sites were dominated by ERE alone (27%) or in combination with other motifs (21%, concomitant presence of multiple motifs) and NR half-sites (14%) (Figure 5A,B). MCF-7-specific ER $\alpha$  binding sites showed a similar motif distribution but had a considerably higher proportion of NR half-sites (24%) and other motifs (29%). Alternatively, in Ishikawa cells, compared to ERE, TEAD (15%), TCF (10%), and NR half motifs (15%) dominated (Figure 5A,B). Notably, Ishikawa-specific SEs were typically bound by ER $\alpha$  at EREs not only in Ishikawa but also in MCF-7 cells, whereas MCF-7-specific SEs were poorly bound in Ishikawa cells (Supplementary Figure S6A,B). This result is consistent with the notion that while ER $\alpha$  is dominantly recruited to EREs or NR half-sites in MCF-7 cells, in Ishikawa cells ER $\alpha$  can also be recruited by TEAD4 and/or TCF12 (Figure 5A,B).



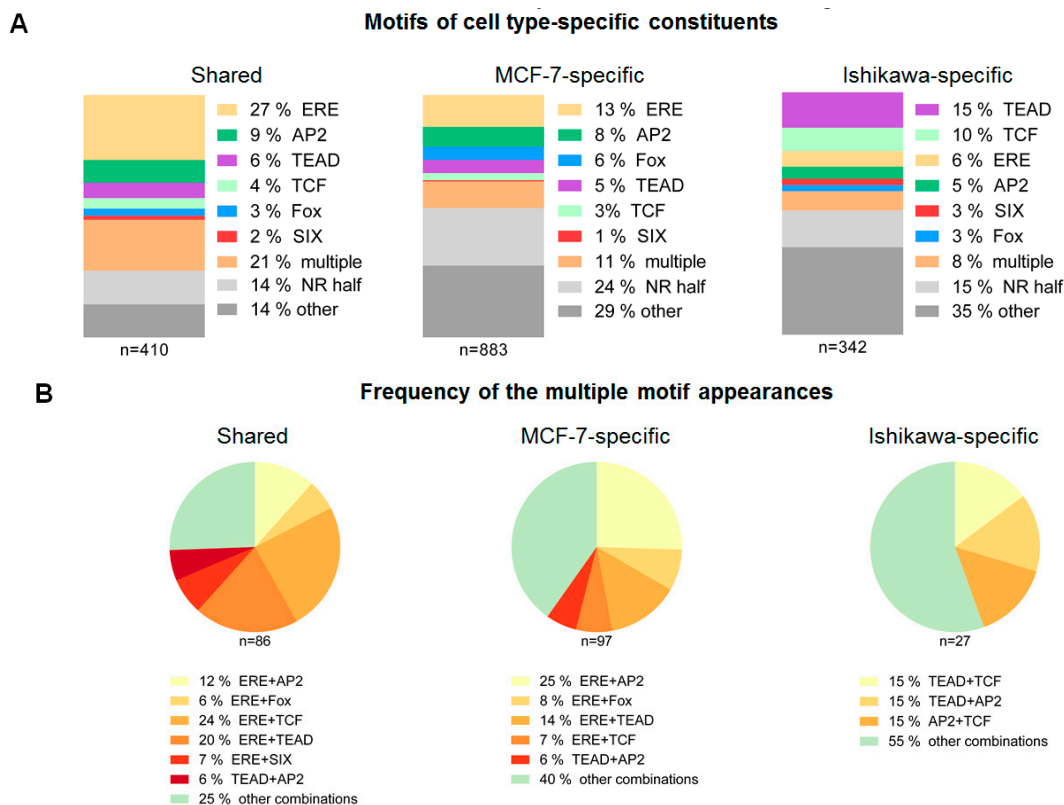


**Figure 5.** Motif composition within the cell line-specific constituents of the 99 shared SE regions. (A) The proportion of investigated DNA motifs within the 99 shared ER $\alpha$ -driven SEs visualized on three bar charts (stacked up to 100%) and classified according to Figure 4B. (B) Pie charts represent the frequency of the top multiple motif appearances defined on panel A.

2.5. Common ER $\alpha$ -driven SEs Generate Similar Transcriptional Output in MCF-7 and Ishikawa Cells

In the next step, we investigated the transcriptional outputs, namely, the maintained expression levels of the genes possibly regulated by cell line-specific and shared SEs identified in both cell lines upon E2 treatment (Ishikawa cells upon 240 min and MCF-7 cells upon 320 min of E2 treatment) (Figure 6A–C).

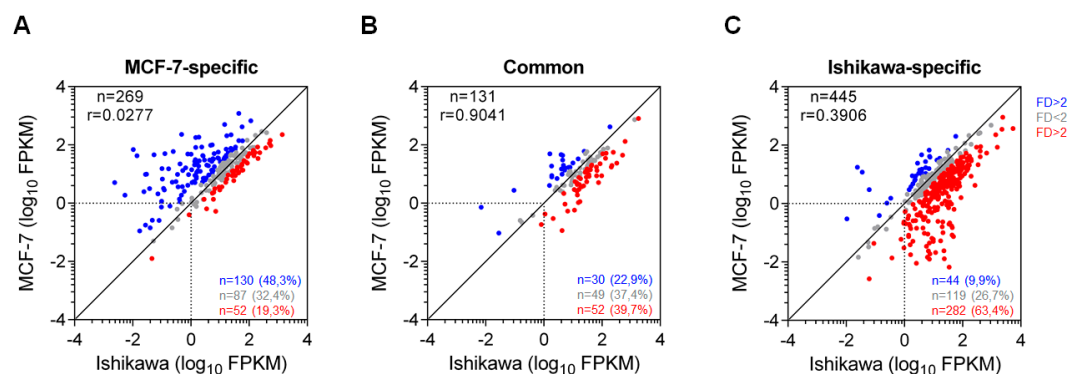


**Figure 6.** Genes regulated by shared SEs show identical expression in MCF-7 and Ishikawa cells. (A–C) Scatter plots showing the expression levels of genes closest to the MCF-7-specific (A), common (B) and Ishikawa-specific (C) ER $\alpha$ -driven SEs. Grey dots represent genes within a 2-fold difference (FD) range between both replicates of MCF-7 and Ishikawa cells; blue and red dots represent genes that exceed this range and are specific to MCF-7 or Ishikawa cells, respectively. The plots contain the number of the genes represented by blue, red or grey dots and the percentage values relative to the total gene number.

Notably, the annotation of regulatory sites to proper genes represents a limitation to any study without using e.g., 3C-based methods, and we did not consider transient gene induction events. According to the main characteristic of SEs (these cause high expression), an asymmetric distribution pattern shifted to MCF-7-specific genes was observed for MCF-7-specific SEs. Nevertheless, several genes showed similar gene expression in both cell lines (<2-fold difference), and a number of genes showed higher expression in Ishikawa cells than in MCF-7 cells (>2-fold difference), although the enhancers' coverage by ER $\alpha$  was not high enough to call them SEs in Ishikawa cells (Figure 6A). The high expression in Ishikawa cells around MCF-7-specific SEs might be due to the presence or absence of different factors (e.g., repressors) or even technical difficulties in SE prediction or gene annotation. A similar phenomenon with an opposite pattern in SE occupancy and gene expression output was also observed for Ishikawa-specific SE-related genes (Figure 6C), genes regulated by shared SEs showed similarly high expression in MCF-7 and Ishikawa cell lines, even though these had largely different sets of collaborative factors (Figure 6B).

### 3. Discussion

As SEs are responsible for cell identity, understanding their mechanism of action is indispensable for improving our knowledge of the regulation of gene expression in general and cellular identity in particular [24]. The recruitment and activation of a dominant TF represents a key step in the formation of SEs, and this recruitment is largely determined by the presence of specific DNA sequences. In addition to these DNA sequences, also known as motifs, which will later result in TF binding, the activating complexes are generated from gathered TFs; moreover, these complexes and protein-DNA interactions are stabilized by additional protein-protein interactions [15].

Previous studies focused mostly on changes in SEs during differentiation; here we examined how SE regions driven by the same master TF behave in two different cancer cell lines. We identified 392 ER $\alpha$ -driven SEs from the breast cancer-derived MCF-7 cells and 618 ER $\alpha$ -driven SEs from the endometrial cancer-derived Ishikawa cells. By examining their unique components, the first evidence was that despite a small overlapping subset, which likely involves conserved binding sites driven by strong EREs, cell type-specific sites indicated the presence of quite different TF binding motifs. These motifs were indeed bound by their recognition proteins, and through protein-protein interactions, some of them have a great affinity for each other. Moreover, certain TF partners might make ER $\alpha$  a hormone-sensitive coregulator, which increases TF binding affinity upon ligand treatment. However, additional investigations using, for example, mass spectrometry, protein interaction assays, and structural biochemical techniques are needed to identify all major components and oligomers of these cell line-specific complexes.

Although in the MCF-7 cell line ER $\alpha$ -dominated SEs are also modulated by the well-known FoxA1 and AP2 $\gamma$  TFs, as described previously, ER $\alpha$  has no coequal TF partner. In Ishikawa cells, we assumed the existence of at least a tripartite protein complex composed of TEAD4, TCF12, FoxM1, or C/EBP $\beta$  in which FoxM1 might have the highest affinity for ER $\alpha$ . However, the role of FoxM1 might be only secondary without its own response elements, and there can be additional TFs playing roles in the assembled regulatory complexes. Of course, the overall structure of a complex based on ChIP-seq data cannot be determined, and further specific experiments supporting this model should be applied. In this study, we carried out a theoretical investigation by using a large publicly available data set derived from two cell lines; however, the proteins identified based on their DNA motifs are indeed parts of a complex acting at SEs and some of them (TEAD4 or TCF12) might have a so-far unknown pioneer role.

Out of the predicted 392 (MCF-7) and 618 (Ishikawa) ER $\alpha$ -driven SEs, only 99 regions overlapped in the two cell lines where ER $\alpha$  was recruited in an alternating fashion, depending on the presence of cell line-specific co-factors and their motif(s). In Ishikawa cells, three-quarters of these ER $\alpha$  binding sites required the presence of at least two collaborative factors. By contrast, in MCF-7 cells, only half of the binding sites showed the presence of both FoxA1 and AP2 $\gamma$  or even TEAD4/TCF12. This observation

may be explained by ER $\alpha$  binding directly to DNA through the ERE, and FoxA1 or AP2 $\gamma$  rather facilitates and/or stabilizes their presence in MCF-7 cells. By contrast, in Ishikawa cells, except for strong canonical EREs, ER $\alpha$  binding occurs almost exclusively through DNA binding collaborating factors. Overall, we observed that depending on the expressed collaborating TFs, ER $\alpha$  behaves in very different ways. One strong ERE might be sufficient for ER $\alpha$  binding but it is basically insufficient for regulation. Nearby motifs—even within the same enhancer or distant ones within the enhancer cluster—will determine the functional ER $\alpha$  TFBSs, and ultimately the whole cistrome. These results explain how gene regulation is carried out by a combination of DNA sequences selected by a combination of expressed TFs. This is a two-level combinatorial code of regulation further supported by specific co-regulators establishing permissive chromatin environment and chromatin interactions.

Overall, the results confirm the importance of the examined SE-bound genomic regions and the genes affected by them. MCF-7-specific ER $\alpha$ -driven SEs indeed regulated genes with pivotal roles in breast cancer (e.g., *BCAS3*, as an amplified and overexpressed gene and *ZNF217*, the candidate organizer of repressive histone modifiers) (highlighted in blue in Supplementary Figure S7A) and altered the expression of genes regulated by Ishikawa-specific SEs, which were typically specific for endometrial cancer (e.g., *ANXA2* and *ATF4*) (highlighted in red in Supplementary Figure S7B) [48–51]. However, some genes were not specifically associated with these two tumor types, but it may be assumed that these play important roles as they are regulated by SEs. Importantly, the genes regulated by common SEs showed similar expression patterns in both MCF-7 and Ishikawa cells even though these were supported by different collaborating factors and most of these commonly regulated genes are associated with poor prognosis or metastatic conditions (e.g., *AZIN1*, *KRT8*, *KRT19*, *SLC9A3R1*, *HES1*, and *CXXC5*), further demonstrating the importance of understanding the function of strong/canonical regulatory elements or complete units, such as SEs (highlighted in grey in Supplementary Figure S7C) [52–54]. Our results suggest that cell type-specific SEs regulate genes with high expression levels, and most of these are indeed linked to (breast and/or endometrial) cancerous processes. Furthermore, the complete or partial deletion of these units may influence the expression of oncogenes so these can be targets of future investigations.

Although several studies reported that different cell types had different transcription profiles and specific TF pools, the essence of our hypothesis is that in different cell types, shared SEs can generate very similar transcriptional events even though these shared SEs are built from various individual enhancers based on the cell type-specific TF profile. Our proposal is that these shared SEs have DNA-encoded responsiveness towards different subsets of TFs, and these behave like *bona fide* multi-tools of the genome.

Our study has several limitations. The results rely on the super-enhancer-regulated genomic regions, not the whole genome is studied; and the cancer cell lines used for the study are not tested to copy number alterations. In addition, instead of early and transient gene expression changes that are difficult to handle, we focused on maintained, steady-state gene expression levels upon a longer period of time in both cell lines. In order to verify the presented cell-type-specific protein-protein interactions further biochemical and genomic methods are required. One of the major limitations of the study is that our bioinformatic investigations were performed on breast- and endometrial cancer cell lines. For a better understanding of the tissue specificity of SEs, animal studies would be needed.

Besides the limitations highlighted, we believe that our investigations provide a new level of understanding of the plasticity of transcription regulation with potential clinical implications. Based on the presented results, further investigations can be initiated that could widen our understanding of the effects and side-effects of hormonal treatments in these two endocrine dependent tissues, namely breast and endometrium, both of these being of major interest in women's health.

## 4. Materials and Methods

### 4.1. Data Selection

Raw ChIP-seq, DNase-seq, and RNA-seq data were downloaded from the Gene Expression Omnibus (GEO). As we used data from ECC-1 isolates of ATCC (American Type Culture Collection, Manassas, VA, USA) that were genotyped as Ishikawa cells [55]; we therefore referred to them as Ishikawa cells. Detailed information about the selected data (including GEO identifiers and references for the publications where these were first published) is included in Supplementary Table S1A–C.

### 4.2. ChIP-seq Analysis

Raw sequence data were analyzed uniformly with an updated version of our previously published computational pipeline [56] as follows: raw sequence reads were aligned to the hg19 reference genome assembly (GRCh37) by using the Burrows-Wheeler Alignment (BWA) tool (v07.10) [57], then BAM files were generated with SAMtools (v0.1.19) [58]. Coverage files were created by the *makeUCSCfile.pl* script of the Hypergeometric Optimization of Motif Enrichment (HOMER) package (v4.2) [59], and peaks were predicted using the Model-based Analysis of ChIP-Seq (MACS2) tool (v2.0.10) with *-callpeak* parameter [60]. In order to remove the artifacts from the predicted peaks, we used the blacklisted genomic regions of the Encyclopedia of DNA Elements (ENCODE) [61].

Reads Per Kilobase per Million mapped reads (RPKM) values were calculated on the  $\pm 50$ -bp regions relative to the peak summits by using the *coverageBed* program of BedTools (v2.23.0) [62]. The number of overlapping peaks and regions was defined by using the DiffBind package (v1.2.4) in R [63]. Read distribution (RD) heat maps were generated by *annotatePeaks.pl* with *-hist 50* and *-ghist* parameters (HOMER). Coverage values for average protein density heat maps were calculated on the summit positions of the RD plots.

### 4.3. Super-Enhancer Prediction

Super-enhancers were predicted from the E2-treated ER $\alpha$  ChIP-seq samples applying the HOMER's *findPeaks.pl* script and the *-style super* parameter. In order to generate a "super-enhancer plot", we used the *-superSlope -1000* parameter and the thus generated "Normalized Tag Count" values were plotted. Tag counts (rpm/bp; reads per million per base pair) of the ER $\alpha$  (super-)enhancers were ranked by their ChIP-seq coverage. The definition of super-enhancers was based on the original strategy, where the outstandingly "active" enhancers or broader regions in which enhancers are closer than 12.5 kb to each other are over slope 1 in the rank order.

### 4.4. Motif Analysis

Motif enrichment analysis was carried out by the *findMotifsGenome.pl* script of HOMER. It was performed on the  $\pm 100$  bp flanking regions of the peak summits. The lengths for the motif search were 10, 12, 14, and 16 bp. *p*-values were calculated by comparing the enrichment within the target regions and that of a random set of regions (background) generated by HOMER.

For the motif distribution plot, motif matrices (shown in Supplementary Figure S2A) were mapped in 30-bp windows within 1.5-kb frames relative to the ER $\alpha$  peak summits using *annotatePeaks.pl* with *-mbed* parameter, BEDtools, and other command-line programs. The clustering of motif distribution patterns was done by Cluster 3.0. The top motif score for each examined region was determined by *annotatePeaks.pl* with *-mscore* parameter. Thresholds of the plotted scores were selected before the last markedly high peak of the motif score distribution.

### 4.5. DNase-seq Analysis

The primary analysis of DNase-seq data was carried out as described for ChIP-seq data analysis.

#### 4.6. RNA-seq Analysis

Raw sequence reads were aligned to the hg19 reference genome assembly (GRCh37) by using TopHat (v2.0.7). The Fragments Per Kilobase of transcript per Million mapped reads (FPKM) values were calculated by Cufflinks (v2.0.2) with default parameters [64].

#### 4.7. Gene Annotation

Super-enhancers were extended to  $\pm 100$ -kb relative to their center. The highest expressed protein-coding gene (at 240 and 320 min of E2 treatment of Ishikawa and MCF-7 cells, respectively) the promoter of which overlapped with an extended region was assigned to the related super-enhancer. If an extended region could not be annotated to any gene, the closest protein-coding gene with at least 1 FPKM expression value was assigned to it by using the PeakAnnotator program [65].

#### 4.8. Visualization

Read distribution, average protein density, and correlation heat maps were plotted by Java TreeView (v1.1.6r4) [66]. Area-proportional Venn diagrams were produced by BioVenn [67]. Box plots, scatter plots, bar charts, and histograms were created with GraphPad Prism 6. Coverage files were visualized by Integrative Genomics Viewer v2.4.16 (IGV) [68].

**Supplementary Materials:** Supplementary materials can be found at <http://www.mdpi.com/1422-0067/21/5/1630/s1>.

**Author Contributions:** B.L.B., D.B., and G.N. designed the study. D.B. collected and analysed the data. D.B. and G.N. carried out the detailed computational analysis and wrote the manuscript. B.L.B. revised the analysis and wrote the manuscript, and all authors have read and agreed to the published version of the manuscript.

**Funding:** This work is supported by the internal research funding provided by the Department of Biochemistry and Molecular Biology, University of Debrecen, Debrecen, Hungary. BLB is supported by the MOLMEDEX FUN-OMICS (GINOP-2.3.3-15-2016-00007) and Debrecen Venture Catapult Program (EFOP-3.6.1-16-2016-00022) grants implemented through the New Hungary Development Plan co-financed by the European Social Fund and the European Regional Development Fund and by the Hungarian Scientific Research Fund (NKFIH OTKA) K 129166. D.B. is supported by the ÚNKP-17-3-IV-DE-140 and ÚNKP-18-3-III-DE-253 New National Excellence Program of the Ministry of Human Capacities and by the EFOP-3.6.3-VEKOP-16-2017-00009 grant. G.N. is supported by the Hungarian Scientific Research Fund (OTKA) PD 124843, by the János Bolyai Research Scholarship of the Hungarian Academy of Sciences and by the ÚNKP-19-4-DE-173 New National Excellence Program of the Ministry of Human Capacities. The authors acknowledge the support of ELIXIR Hungary ([www.elixir-hungary.org](http://www.elixir-hungary.org)). This study makes use of publicly-available sequencing data, which were cited in the manuscript.

**Acknowledgments:** The authors would like to thank István Szatmári for critical revision and comments on the manuscript, Nature Research Editing Service for the language editing, and Balázs Venkovits (Institute of English and American Studies, University of Debrecen, Hungary) for proofreading the manuscript prior to submission.

**Conflicts of Interest:** The authors declare no conflict of interest.

#### Abbreviations

ER $\alpha$	estrogen receptor alpha
ERE	estrogen response element
E2	estradiol (17 $\beta$ -estradiol)
H3K27ac	acetylation at the 27th lysine residue of the histone H3 protein
NR	nuclear receptor
SE	super-enhancer
TF	transcription factor
TFBS	transcription factor binding site

## References

1. Germain, P.; Staels, B.; Dacquet, C.; Spedding, M.; Laudet, V. Overview of nomenclature of nuclear receptors. *Pharmacol. Rev.* **2006**, *58*, 685–704. [[CrossRef](#)] [[PubMed](#)]
2. Ross-Innes, C.S.; Stark, R.; Teschendorff, A.E.; Holmes, K.A.; Ali, H.R.; Dunning, M.J.; Brown, G.D.; Gojis, O.; Ellis, I.O.; Green, A.R.; et al. Differential oestrogen receptor binding is associated with clinical outcome in breast cancer. *Nature* **2012**, *481*, 389–393. [[CrossRef](#)] [[PubMed](#)]
3. Zhang, Y.; Zhao, D.; Gong, C.; Zhang, F.; He, J.; Zhang, W.; Zhao, Y.; Sun, J. Prognostic role of hormone receptors in endometrial cancer: A systematic review and meta-analysis. *World J. Surg. Oncol.* **2015**, *13*, 208. [[CrossRef](#)] [[PubMed](#)]
4. Reed, B.G.; Carr, B.R. *The Normal Menstrual Cycle and the Control of Ovulation*; MDText.com Inc.: South Dartmouth, MA, USA, 2000.
5. Väänänen, H.K.; Härkönen, P.L. Estrogen and bone metabolism. *Maturitas* **1996**, *23*, S65–S69. [[CrossRef](#)]
6. Groothuis, P.G.; Dassen, H.H.N.M.; Romano, A.; Punyadeera, C. Estrogen and the endometrium: Lessons learned from gene expression profiling in rodents and human. *Hum. Reprod. Update* **2007**, *13*, 405–417. [[CrossRef](#)] [[PubMed](#)]
7. Klein-Hitpass, L.; Schorpp, M.; Wagner, U.; Ryffel, G.U. An estrogen-responsive element derived from the 5' flanking region of the *Xenopus vitellogenin A2* gene functions in transfected human cells. *Cell* **1986**, *46*, 1053–1061. [[CrossRef](#)]
8. Kumar, V.; Chambon, P. The estrogen receptor binds tightly to its responsive element as a ligand-induced homodimer. *Cell* **1988**, *55*, 145–156. [[CrossRef](#)]
9. Klinge, C.M. Estrogen receptor interaction with co-activators and co-repressors. *Steroids* **2000**, *65*, 227–251. [[CrossRef](#)]
10. Gaub, M.P.; Bellard, M.; Scheuer, I.; Chambon, P.; Sassone-Corsi, P. Activation of the ovalbumin gene by the estrogen receptor involves the fos-jun complex. *Cell* **1990**, *63*, 1267–1276. [[CrossRef](#)]
11. Klinge, C.M. Estrogen receptor interaction with estrogen response elements. *Nucleic Acids Res.* **2001**, *29*, 2905–2919. [[CrossRef](#)]
12. Vega, V.B.; Lin, C.-Y.; Lai, K.S.; Kong, S.L.; Xie, M.; Su, X.; Teh, H.F.; Thomsen, J.S.; Yeo, A.L.; Sung, W.K.; et al. Multiplatform genome-wide identification and modeling of functional human estrogen receptor binding sites. *Genome Biol.* **2006**, *7*, R82. [[CrossRef](#)] [[PubMed](#)]
13. Joseph, R.; Orlov, Y.L.; Huss, M.; Sun, W.; Kong, S.L.; Ukil, L.; Pan, Y.F.; Li, G.; Lim, M.; Thomsen, J.S.; et al. Integrative model of genomic factors for determining binding site selection by estrogen receptor- $\alpha$ . *Mol. Syst. Biol.* **2010**, *6*, 456. [[CrossRef](#)] [[PubMed](#)]
14. Bourdeau, V.; Deschênes, J.; Métivier, R.; Nagai, Y.; Nguyen, D.; Bretschneider, N.; Gannon, F.; White, J.H.; Mader, S. Genome-wide identification of high-affinity estrogen response elements in human and mouse. *Mol. Endocrinol.* **2004**, *18*, 1411–1427. [[CrossRef](#)] [[PubMed](#)]
15. Bojcsuk, D.; Nagy, G.; Balint, B.L. Inducible super-enhancers are organized based on canonical signal-specific transcription factor binding elements. *Nucleic Acids Res.* **2017**, *45*, 3699–3706. [[CrossRef](#)]
16. Bojcsuk, D.; Bálint, B.L. Classification of different types of estrogen receptor alpha binding sites in MCF-7 cells. *J. Biotechnol.* **2019**, *299*, 13–20. [[CrossRef](#)]
17. Lovén, J.; Hoke, H.A.; Lin, C.Y.; Lau, A.; Orlando, D.A.; Vakoc, C.R.; Bradner, J.E.; Lee, T.I.; Young, R.A. Selective inhibition of tumor oncogenes by disruption of super-enhancers. *Cell* **2013**, *153*, 320–334. [[CrossRef](#)]
18. Pott, S.; Lieb, J.D. What are super-enhancers? *Nat. Genet.* **2015**, *47*, 8–12. [[CrossRef](#)]
19. Kagey, M.H.; Newman, J.J.; Bilodeau, S.; Zhan, Y.; Orlando, D.A.; van Berkum, N.L.; Ebmeier, C.C.; Goossens, J.; Rahl, P.B.; Levine, S.S.; et al. Mediator and cohesin connect gene expression and chromatin architecture. *Nature* **2010**, *467*, 430–435. [[CrossRef](#)]
20. Di Micco, R.; Fontanals-Cirera, B.; Low, V.; Ntziachristos, P.; Yuen, S.K.; Lovell, C.D.; Dolgalev, I.; Yonekubo, Y.; Zhang, G.; Rusinova, E.; et al. Control of embryonic stem cell identity by BRD4-dependent transcriptional elongation of super-enhancer-associated pluripotency genes. *Cell Rep.* **2014**, *9*, 234–247. [[CrossRef](#)]
21. Tsai, C.-J.; Nussinov, R. Gene-specific transcription activation via long-range allosteric shape-shifting. *Biochem. J.* **2011**, *439*, 15–25. [[CrossRef](#)]

22. Sabari, B.R.; Dall'Agnese, A.; Boija, A.; Klein, I.A.; Coffey, E.L.; Shrinivas, K.; Abraham, B.J.; Hannett, N.M.; Zamudio, A.V.; Manteiga, J.C.; et al. Coactivator condensation at super-enhancers links phase separation and gene control. *Science* **2018**, *361*, eaar3958. [[CrossRef](#)] [[PubMed](#)]
23. Hnisz, D.; Shrinivas, K.; Young, R.A.; Chakraborty, A.K.; Sharp, P.A. A phase separation model for transcriptional control. *Cell* **2017**, *169*, 13–23. [[CrossRef](#)] [[PubMed](#)]
24. Hnisz, D.; Abraham, B.J.; Lee, T.I.; Lau, A.; Saint-André, V.; Sigova, A.A.; Hoke, H.A.; Young, R.A. Super-enhancers in the control of cell identity and disease. *Cell* **2013**, *155*, 934–947. [[CrossRef](#)] [[PubMed](#)]
25. Siersbæk, R.; Baek, S.; Rabiee, A.; Nielsen, R.; Traynor, S.; Clark, N.; Sandelin, A.; Jensen, O.N.; Sung, M.-H.; Hager, G.L.; et al. Molecular architecture of transcription factor hotspots in early adipogenesis. *Cell Rep.* **2014**, *7*, 1434–1442. [[CrossRef](#)] [[PubMed](#)]
26. Willi, M.; Yoo, K.H.; Reinisch, F.; Kuhns, T.M.; Lee, H.K.; Wang, C.; Hennighausen, L. Facultative CTCF sites moderate mammary super-enhancer activity and regulate juxtaposed gene in non-mammary cells. *Nat. Commun.* **2017**, *8*, 16069. [[CrossRef](#)]
27. Downen, J.M.; Fan, Z.P.; Hnisz, D.; Ren, G.; Abraham, B.J.; Zhang, L.N.; Weintraub, A.S.; Schuijers, J.; Lee, T.I.; Zhao, K.; et al. Control of cell identity genes occurs in insulated neighborhoods in mammalian chromosomes. *Cell* **2014**, *159*, 374–387. [[CrossRef](#)]
28. Shin, H.Y. Targeting super-enhancers for disease treatment and diagnosis. *Mol. Cells* **2018**, *41*, 506–514.
29. Sengupta, S.; George, R.E. Super-enhancer-driven transcriptional dependencies in cancer. *Trends Cancer* **2017**, *3*, 269–281. [[CrossRef](#)]
30. Huang, J.; Li, K.; Cai, W.; Liu, X.; Zhang, Y.; Orkin, S.H.; Xu, J.; Yuan, G.-C. Dissecting super-enhancer hierarchy based on chromatin interactions. *Nat. Commun.* **2018**, *9*, 943. [[CrossRef](#)]
31. Nord, A.S.; Blow, M.J.; Attanasio, C.; Akiyama, J.A.; Holt, A.; Hosseini, R.; Phouanavong, S.; Plajzer-Frick, I.; Shoukry, M.; Afzal, V.; et al. Rapid and pervasive changes in genome-wide enhancer usage during mammalian development. *Cell* **2013**, *155*, 1521–1531. [[CrossRef](#)]
32. Carroll, J.S.; Liu, X.S.; Brodsky, A.S.; Li, W.; Meyer, C.A.; Szary, A.J.; Eeckhoutte, J.; Shao, W.; Hestermann, E.V.; Geistlinger, T.R.; et al. Chromosome-wide mapping of estrogen receptor binding reveals long-range regulation requiring the forkhead protein FoxA1. *Cell* **2005**, *122*, 33–43. [[CrossRef](#)] [[PubMed](#)]
33. Hurtado, A.; Holmes, K.A.; Ross-Innes, C.S.; Schmidt, D.; Carroll, J.S. FoxA1 is a key determinant of estrogen receptor function and endocrine response. *Nat. Genet.* **2011**, *43*, 27–33. [[CrossRef](#)] [[PubMed](#)]
34. Tan, S.K.; Lin, Z.H.; Chang, C.W.; Varang, V.; Chng, K.R.; Pan, Y.F.; Yong, E.L.; Sung, W.K.; Sung, W.K.; Cheung, E. AP-2 $\gamma$  regulates oestrogen receptor-mediated long-range chromatin interaction and gene transcription. *EMBO J.* **2011**, *30*, 2569–2581. [[CrossRef](#)] [[PubMed](#)]
35. Ross-Innes, C.S.; Stark, R.; Holmes, K.A.; Schmidt, D.; Spyrou, C.; Russell, R.; Massie, C.E.; Vowler, S.L.; Eldridge, M.; Carroll, J.S. Cooperative interaction between retinoic acid receptor- and estrogen receptor in breast cancer. *Genes Dev.* **2010**, *24*, 171–182. [[CrossRef](#)] [[PubMed](#)]
36. Theodorou, V.; Stark, R.; Menon, S.; Carroll, J.S. GATA3 acts upstream of FOXA1 in mediating ESR1 binding by shaping enhancer accessibility. *Genome Res.* **2013**, *23*, 12–22. [[CrossRef](#)] [[PubMed](#)]
37. Liu, Z.; Merkurjev, D.; Yang, F.; Li, W.; Oh, S.; Friedman, M.J.; Song, X.; Zhang, F.; Ma, Q.; Ohgi, K.A.; et al. Enhancer activation requires trans-recruitment of a mega transcription factor complex. *Cell* **2014**, *159*, 358–373. [[CrossRef](#)] [[PubMed](#)]
38. Droog, M.; Nevedomskaya, E.; Kim, Y.; Severson, T.; Flach, K.D.; Opdam, M.; Schuurman, K.; Gradowska, P.; Hauptmann, M.; Dackus, G.; et al. Comparative cistromics reveals genomic cross-talk between FoxA1 and ER in tamoxifen-associated endometrial carcinomas. *Cancer Res.* **2016**, *76*, 3773–3784. [[CrossRef](#)]
39. Khushi, M.; Clarke, C.L.; Graham, J.D. Bioinformatic analysis of cis-regulatory interactions between progesterone and estrogen receptors in breast cancer. *Peer J.* **2014**, *2*, e654. [[CrossRef](#)]
40. Liu, X.; Li, H.; Rajurkar, M.; Li, Q.; Cotton, J.L.; Ou, J.; Zhu, L.J.; Goel, H.L.; Mercurio, A.M.; Park, J.-S.; et al. Tead and AP1 coordinate transcription and motility. *Cell Rep.* **2016**, *14*, 1169–1180. [[CrossRef](#)]
41. Chen, Q.; Liang, Y.; Zhang, Y.; Jiang, M.; Han, Z.; Liang, Y.; Wan, Y.; Yin, J.; He, H.-C.; Zhong, W. Decreased expression of TCF12 contributes to progression and predicts biochemical recurrence in patients with prostate cancer. *Tumor Biol.* **2017**, *39*, 101042831770392. [[CrossRef](#)]
42. Kompass, K.S.; Witte, J.S. Co-regulatory expression quantitative trait loci mapping: Method and application to endometrial cancer. *BMC Med. Genom.* **2011**, *4*, 6. [[CrossRef](#)] [[PubMed](#)]

43. Suen, A.A.; Jefferson, W.N.; Wood, C.E.; Padilla-Banks, E.; Bae-Jump, V.L.; Williams, C.J. SIX1 oncoprotein as a biomarker in a model of hormonal carcinogenesis and in human endometrial cancer. *Mol. Cancer Res.* **2016**, *14*, 849–858. [[CrossRef](#)] [[PubMed](#)]
44. Stender, J.D.; Kim, K.; Charn, T.H.; Komm, B.; Chang, K.C.N.; Kraus, W.L.; Benner, C.; Glass, C.K.; Katzenellenbogen, B.S. Genome-wide analysis of estrogen receptor alpha DNA binding and tethering mechanisms identifies Runx1 as a novel tethering factor in receptor-mediated transcriptional activation. *Mol. Cell. Biol.* **2010**, *30*, 3943–3955. [[CrossRef](#)] [[PubMed](#)]
45. Lupien, M.; Eeckhoutte, J.; Meyer, C.A.; Wang, Q.; Zhang, Y.; Li, W.; Carroll, J.S.; Liu, X.S.; Brown, M. FoxA1 translates epigenetic Signatures into enhancer-driven lineage-specific transcription. *Cell* **2008**, *132*, 958–970. [[CrossRef](#)] [[PubMed](#)]
46. Tewari, A.K.; Yardimci, G.; Shibata, Y.; Sheffield, N.C.; Song, L.; Taylor, B.S.; Georgiev, S.G.; Coetzee, G.A.; Ohler, U.; Furey, T.S.; et al. Chromatin accessibility reveals insights into androgen receptor activation and transcriptional specificity. *Genome Biol.* **2012**, *13*, R88. [[CrossRef](#)] [[PubMed](#)]
47. Sahu, B.; Laakso, M.; Pihlajamaa, P.; Ovaska, K.; Sinielnikov, I.; Hautaniemi, S.; Janne, O.A. FoxA1 Specifies unique androgen and glucocorticoid receptor binding events in prostate cancer cells. *Cancer Res.* **2013**, *73*, 1570–1580. [[CrossRef](#)]
48. Bärlund, M.; Monni, O.; Weaver, J.D.; Kauraniemi, P.; Sauter, G.; Heiskanen, M.; Kallioniemi, O.-P.; Kallioniemi, A. Cloning of BCAS3 (17q23) and BCAS4 (20q13) genes that undergo amplification, overexpression, and fusion in breast cancer†. *Genes Chromosom. Cancer* **2002**, *35*, 311–317. [[CrossRef](#)]
49. Vendrell, J.A.; Thollet, A.; Nguyen, N.T.; Ghayad, S.E.; Vinot, S.; Bieche, I.; Grisard, E.; Jossierand, V.; Coll, J.-L.; Roux, P.; et al. ZNF217 is a marker of poor prognosis in breast cancer that drives epithelial-mesenchymal transition and invasion. *Cancer Res.* **2012**, *72*, 3593–3606. [[CrossRef](#)]
50. Alonso-Alconada, L.; Santacana, M.; Garcia-Sanz, P.; Muinelto-Romay, L.; Colas, E.; Mirantes, C.; Monge, M.; Cueva, J.; Oliva, E.; Soslow, R.A.; et al. Annexin-A2 as predictor biomarker of recurrent disease in endometrial cancer. *Int. J. Cancer* **2015**, *136*, 1863–1873. [[CrossRef](#)]
51. Liu, B.; Chen, P.; Xi, D.; Zhu, H.; Gao, Y. ATF4 regulates CCL2 expression to promote endometrial cancer growth by controlling macrophage infiltration. *Exp. Cell Res.* **2017**, *360*, 105–112. [[CrossRef](#)]
52. Silva, T.M.; Cirenajwis, H.; Wallace, H.M.; Oredsson, S.; Persson, L. A role for antizyme inhibitor in cell proliferation. *Amino. Acids* **2015**, *47*, 1341–1352. [[CrossRef](#)] [[PubMed](#)]
53. Fang, L.; Wang, Y.; Gao, Y.; Chen, X. Overexpression of CXXC5 is a strong poor prognostic factor in ER+ breast cancer. *Oncol. Lett.* **2018**, *16*, 395–401. [[CrossRef](#)] [[PubMed](#)]
54. Tomaskovic-Crook, E.; Thompson, E.W.; Thiery, J.P. Epithelial to mesenchymal transition and breast cancer. *Breast Cancer Res.* **2009**, *11*, 213. [[CrossRef](#)] [[PubMed](#)]
55. Korch, C.; Spillman, M.A.; Jackson, T.A.; Jacobsen, B.M.; Murphy, S.K.; Lessey, B.A.; Jordan, V.C.; Bradford, A.P. DNA profiling analysis of endometrial and ovarian cell lines reveals misidentification, redundancy and contamination. *Gynecol. Oncol.* **2012**, *127*, 241–248. [[CrossRef](#)] [[PubMed](#)]
56. Barta, E. Command line analysis of ChIP-seq results. *EMB Net. J.* **2011**, *17*, 13–17. [[CrossRef](#)]
57. Li, H.; Durbin, R. Fast and accurate short read alignment with Burrows-Wheeler transform. *Bioinformatics* **2009**, *25*, 1754–1760. [[CrossRef](#)]
58. Li, H.; Handsaker, B.; Wysoker, A.; Fennell, T.; Ruan, J.; Homer, N.; Marth, G.; Abecasis, G.; Durbin, R. 1000 genome project data processing subgroup the sequence alignment/map format and SAMtools. *Bioinformatics* **2009**, *25*, 2078–2079. [[CrossRef](#)]
59. Heinz, S.; Benner, C.; Spann, N.; Bertolino, E.; Lin, Y.C.; Laslo, P.; Cheng, J.X.; Murre, C.; Singh, H.; Glass, C.K. Simple combinations of lineage-determining transcription factors prime cis-regulatory elements required for macrophage and B cell identities. *Mol. Cell* **2010**, *38*, 576–589. [[CrossRef](#)]
60. Zhang, Y.; Liu, T.; Meyer, C.A.; Eeckhoutte, J.; Johnson, D.S.; Bernstein, B.E.; Nusbaum, C.; Myers, R.M.; Brown, M.; Li, W.; et al. Model-based analysis of ChIP-Seq (MACS). *Genome Biol.* **2008**, *9*, R137. [[CrossRef](#)]
61. Dunham, I.; Kundaje, A.; Aldred, S.F.; Collins, P.J.; Davis, C.A.; Doyle, F.; Epstein, C.B.; Frietze, S.; Harrow, J.; Kaul, R.; et al. An integrated encyclopedia of DNA elements in the human genome. *Nature* **2012**, *489*, 57–74.
62. Quinlan, A.R.; Hall, I.M. BEDTools: A flexible suite of utilities for comparing genomic features. *Bioinformatics* **2010**, *26*, 841–842. [[CrossRef](#)] [[PubMed](#)]

63. Stark, R.; Brown, G. DiffBind: Differential Binding Analysis of ChIP-Seq Peak Data. Available online: <https://bioconductor.statistik.tu-dortmund.de/packages/2.13/bioc/vignettes/DiffBind/inst/doc/DiffBind.pdf> (accessed on 22 February 2020).
64. Trapnell, C.; Williams, B.A.; Pertea, G.; Mortazavi, A.; Kwan, G.; van Baren, M.J.; Salzberg, S.L.; Wold, B.J.; Pachter, L. Transcript assembly and quantification by RNA-Seq reveals unannotated transcripts and isoform switching during cell differentiation. *Nat. Biotechnol.* **2010**, *28*, 511–515. [[CrossRef](#)] [[PubMed](#)]
65. Salmon-Divon, M.; Dvinge, H.; Tammoja, K.; Bertone, P. PeakAnalyzer: Genome-wide annotation of chromatin binding and modification loci. *BMC Bioinform.* **2010**, *11*, 415. [[CrossRef](#)] [[PubMed](#)]
66. Saldanha, A.J. Java Treeview—Extensible visualization of microarray data. *Bioinformatics* **2004**, *20*, 3246–3248. [[CrossRef](#)] [[PubMed](#)]
67. Hulsen, T.; de Vlieg, J.; Alkema, W. BioVenn—A web application for the comparison and visualization of biological lists using area-proportional Venn diagrams. *BMC Genom.* **2008**, *9*, 488. [[CrossRef](#)] [[PubMed](#)]
68. Thorvaldsdottir, H.; Robinson, J.T.; Mesirov, J.P. Integrative genomics viewer (IGV): High-performance genomics data visualization and exploration. *Brief. Bioinform.* **2013**, *14*, 178–192. [[CrossRef](#)] [[PubMed](#)]



© 2020 by the authors. Licensee MDPI, Basel, Switzerland. This article is an open access article distributed under the terms and conditions of the Creative Commons Attribution (CC BY) license (<http://creativecommons.org/licenses/by/4.0/>).